Orometry-based Terrain Analysis and Synthesis

OSCAR ARGUDO, Univ Lyon, Université Lyon 1, CNRS, LIRIS, France
ERIC GALIN, Univ Lyon, Université Lyon 1, CNRS, LIRIS, France
ADRIEN PEYTAVIE, Univ Lyon, Université Lyon 1, CNRS, LIRIS, France
AXEL PARIS, Univ Lyon, Université Lyon 1, CNRS, LIRIS, France
JAMES GAIN, University of Cape Town, South Africa
ERIC GUÉRIN, Univ Lyon, INSA-Lyon, CNRS, LIRIS, France

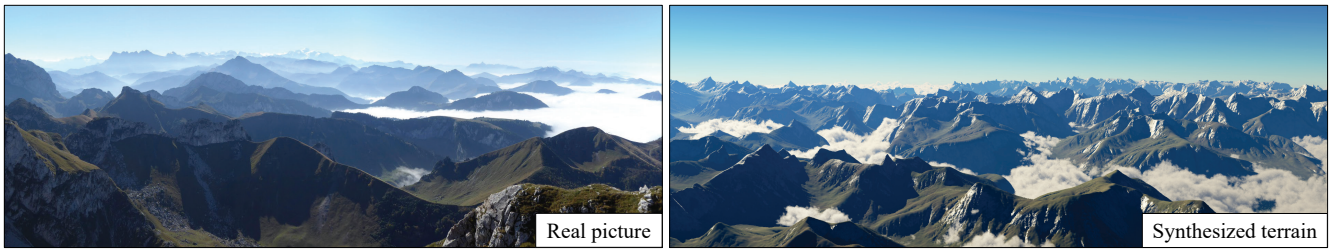

Fig. 1. Given a regional terrain type and a rough elevation control map as input, our method automatically generates a synthetic graph of connected peaks and saddles, which is, in turn, used to procedurally generate a detailed heightfield obeying the orometric properties of the prescribed terrain type.

Mountainous digital terrains are an important element of many virtual environments and find application in games, film, simulation and training. Unfortunately, while existing synthesis methods produce locally plausible results they often fail to respect global structure. This is exacerbated by a dearth of automated metrics for assessing terrain properties at a macro level.

We address these issues by building on techniques from orometry, a field that involves the measurement of mountains and other relief features. First, we construct a sparse metric computed on the peaks and saddles of a mountain range and show that, when used for classification, this is capable of robustly distinguishing between different mountain ranges. Second, we present a synthesis method that takes a coarse elevation map as input and builds a graph of peaks and saddles respecting a given orometric distribution. This is then expanded into a fully continuous elevation function by deriving a consistent river network and shaping the valley slopes. In terms of authoring, users provide various control maps and are also able to edit, reposition, insert and remove terrain features all while retaining the characteristics of a selected mountain range.

The result is a terrain analysis and synthesis method that considers and incorporates orometric properties, and is, on the basis of our perceptual study, more visually plausible than existing terrain generation methods.

Authors' addresses: Oscar Argudo, Univ Lyon, Université Lyon 1, CNRS, LIRIS, France, oscar.argudo@liris.cnrs.fr; Eric Galin, Univ Lyon, Université Lyon 1, CNRS, LIRIS, France, eric.galin@liris.cnrs.fr; Adrien Peytavie, Univ Lyon, Université Lyon 1, CNRS, LIRIS, France, adrien.peytavie@liris.cnrs.fr; Axel Paris, Univ Lyon, Université Lyon 1, CNRS, LIRIS, France, axel.paris@liris.cnrs.fr; James Gain, University of Cape Town, South Africa, jgain@cs.uct.ac.za; Eric Guérin, Univ Lyon, INSA-Lyon, CNRS, LIRIS, France, eric.guerin@liris.cnrs.fr.

0730-0301/2019/11-ART199 $15.00
https://doi.org/10.1145/3355089.3356535

CCS Concepts: • **Computing methodologies** → **Shape modeling**.

Additional Key Words and Phrases: Procedural modeling, terrain generation

ACM Reference Format:
Oscar Argudo, Eric Galin, Adrien Peytavie, Axel Paris, James Gain, and Eric Guérin. 2019. Orometry-based Terrain Analysis and Synthesis. *ACM Trans. Graph.* 38, 6, Article 199 (November 2019), 12 pages. https://doi.org/10.1145/3355089.3356535

1 INTRODUCTION

Mountains and ridges are a visually salient feature in many large-scale digital terrains, and thus serve as a backdrop or key scene element in a range of computer graphics applications. Depending as they do on a variety of geomorphological effects, such as plate tectonics, glaciation, and erosion, it is no surprise that mountain ranges exhibit different characteristics, ranging from the prominent peaks of the Rockies and Swiss Alps to the gentler and more uniform structure of the Appalachians and Scottish Highlands. In particular, relative peak prominence crucially affects the vista from different vantage points on a mountainscape, and is one of the defining characteristics. It is current practice to assess such aspects of digital terrains through visual inspection. Ideally, this should consist of a perceptual study involving dozens of participants with either informal or formal expertise, such as hikers or geomorphologists. Unfortunately, this tends to be both time consuming and expensive, and is generally only applied as a summative rather than formative evaluation. The outcome is that few terrain synthesis methods adequately capture the global properties of mountainous regions.

Fortunately, it is exactly these aspects, namely the statistical interrelationship and relative prominence of peaks and saddles in relief areas, that is the focus of orometry, a subfield of geomorphology dealing with the measurement of mountains. In this paper, we directly apply orometry to improve the realism of virtual terrains.

We begin by compiling an orometric descriptor that considers the distribution of prominence and isolation of peaks, the ridges and saddles connecting them, and the relative orientation of these features. When used for classification this descriptor is able to accurately discriminate between mountain ranges from different geographic regions. Next, we provide an algorithm for the orometric synthesis of terrains by applying the metric directly as an optimization criterion in the construction of a Divide Tree, which represents the sparse placement and interconnection of peaks and saddles. Taking care to respect the orometric constraints, a dual graph is then derived for the placement of river valleys, followed by the introduction of fractal-based detail and an erosion post-process.

The main technical contributions outlined in this paper include: 1) A set of orometric properties that can be derived from an elevation map and then used for accurate mountain range classification. 2) A synthesis method that, given such a set of pre-computed orometric properties, is capable of generating a matching terrain by first constructing a Divide Tree to represent the local connectivity of peaks and saddles, and then populating the map with detail on the basis of a dual river graph and procedural upsampling. 3) The incorporation of a range of authoring mechanisms, which allow both global control (through mountain type and coarse elevation paint maps) and local control (by editing the Divide Tree and terrain features) while retaining an orometric correspondence.

In summary, we present a novel application of orometry to the analysis, classification and synthesis of digital terrains in computer graphics. Our model is the first to capture the vast diversity of mountainous terrain types evident in the world's geography, ranging from rolling hills in geologically stable mountains to smooth Saharan dunes to the delineated peaks of younger mountain ranges. This work not only benefits the entertainment industry, where our synthesis method could be used to generate and combine different terrain classes, but also serves as a first step in analyzing the characteristics of synthetic and real terrains.

2 RELATED WORK

Our approach is to analyse existing real-world source terrains, extract a compact but rich characterization, and synthesize new target terrains matching these source characteristics. Here, we focus on existing terrain generators that either perform synthesis based on a previous analysis, or only require a sparse set of input features. For a more complete coverage of terrain modeling techniques, the reader is referred to the review by Galin *et al.* [2019].

2.1 Generation from analyzed data

For decades, researchers have sought to generate terrains by replicating their visual appearance. Nevertheless, among these, only a few are based on a through-line of analysis, characterization and synthesis from real terrain data sources.

A fundamental property observed in real terrains is their fractal self-similarity [Kelley et al. 1988; Mandelbrot 1982; Musgrave et al. 1989; Prusinkiewicz and Hammel 1993]. However, by nature, terrains are not mono-fractal and so efforts have been made to adapt fractal dimension with respect to elevation, leading to multi-fractal properties [Mandelbrot 1982]. In this vein, Parberry proposed a characterization of terrains according to a histogram of heights [Parberry 2014] and gradients [Parberry 2015], which are then fed into a modified noise generator to produce histogram-matching terrains.

Most recent example-based terrain methods rely on an implicit rather than explicit analysis of terrains. For instance, adaptations of texture synthesis [Gain et al. 2015; Zhou et al. 2007] cut and rejoin terrains at a patch or pixel level, and the analysis involves appropriate matching of user-supplied constraints and joins between seams. Sparse modeling [Argudo et al. 2017; Guérin et al. 2016] also analyzes terrains, but in this case it is in the service of building a reusable dictionary of localised feature patches.

Similar to our approach, the analysis of topological and geometrical features of street networks has proved to be successful for the classification between different cities and their procedural generation [AlHalawani et al. 2014]. Such graph properties are orthogonal to our proposed orometric descriptors, however, which are computed from the elevation of the graph nodes instead.

2.2 Generation from sparse features

There are a number of existing methods capable of synthesizing terrains from a relatively sparse set of vector-based constraints.

Procedural methods are particularly suited to this approach. A common thread is to allow user authoring through a sketching interface that gives rise to sparse curve constraints submitted to a subdivision process [Belhadj 2007], deformed wavelet noise [Gain et al. 2009], or diffusion [Hnaidi et al. 2010]. Genevaux *et al.* [2015] introduce a more generic model for representing complex terrains as a hierarchy of primitives combined with blending operators. This representation has been used in a context similar to ours, where the terrain was generated from its river network [Génevaux et al. 2013].

Erosion simulations are generally much less suited to satisfying vector constraints. Nevertheless, we do end up adapting erosion algorithms so as not to break existing constraints on orometry.

Lastly, in some cases, example-based methods do offer sparse high-level feature controls. Texture-based terrain synthesis [Gain et al. 2015; Zhou et al. 2007] enables a mixture of point, curve and style features, and by using a Generative Adversarial Network, Guérin *et al.* [2017] are able to generate terrain from simple sketches detailing the crest lines and river network. The recent network TileGAN [Frühstück et al. 2019] can synthesize very large terrains from a rough guidance map by tiling a latent space field that produces the final texture when run through the generator. However, training requires thousands of tiles and can last up to a few weeks, making it impractical for using it with several differentiated regions, each requiring a specific intensive training phase. Zhou *et al.* [Zhou et al. 2018] learn global texture structure and patterns from a single image exemplar and replicate them according to a guidance map. While convincing on textures, this approach fails to respect the properties of the exemplar terrain as demonstrated by our experiments.

A pertinent question is whether our orometrically-derived features can be fed into any of these techniques, thereby enabling the back-end of our synthesis algorithm to be replaced. Unfortunately, because our constraints need to be strictly respected, only a subset of techniques are suitable [Belhadj 2007; Gain et al. 2015, 2009; Hnaidi et al. 2010]. Furthermore, unlike our generator, most of these

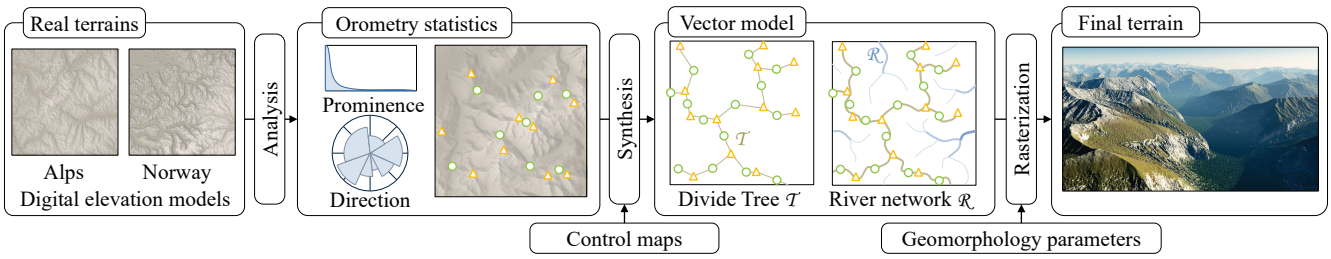

Fig. 2. Synthesis overview: given a set of terrain elevation models and corresponding region labels, we perform an analysis of their orometric statistics, which includes building a Divide Tree connecting peaks and saddles. These statistics are then used to generate a sparse vector representation of synthetic terrains featuring consistent ridge $\mathcal{T}$ and river $\mathcal{R}$ networks, which are fed to noise- and erosion-based rasterization processes to create the final terrain. User-control is incorporated through control maps (specifying peak density and average elevation) during synthesis, and formation parameters during rasterization.

alternatives require a complete set of constraints that include not only peaks and saddles, but also a valley network.

To our knowledge, this work is the first to extract compact defining characteristics from a widely ranging real-world relief and use this as a basis for generating new landscapes.

3 OVERVIEW

Our work is founded on the observation that mountainous regions have highly characteristic peak distributions and branching ridge patterns. On this basis, we analyze the orometric properties of real terrains (Section 4), including the prominence, dominance, isolation, and saddle orientation of their peaks, and use these properties to train a Random Forest classifier that can reliably distinguish between different terrain archetypes. Having demonstrated the utility of an orometric analysis, the next step is to apply the derived statistics to guide terrain synthesis (see Figure 2).

Our terrain synthesis process is organized into two main steps. First, we generate a Divide Tree $\mathcal{T}$ (Section 5), which encodes the layout of peaks, saddles, and ridges, and conforms to provided orometric statistics. Second, we develop this into a fully-realized terrain (Section 6) by forming a river network $\mathcal{R}$ from the dual graph of $\mathcal{T}$, then introducing additional samples on ridges and valley slopes, and finally converting this via Delaunay triangulation into an elevation map to which multi-fractal noise and multi-resolution erosion algorithms can be applied. Throughout this process the positions of peaks and saddles (and thus the terrain orometry) are preserved.

In terms of authoring, the user chooses a particular mountain class to mimic, but can also supply optional peak probability C_P and coarse elevation C_H maps so as to influence the average density and elevation of peaks over the prescribed domain. Furthermore, they are able to place specific peaks and ridges, or even copy and paste subparts of a previously authored or real-world Divide Tree.

4 OROMETRY

Orometry is central to our approach and provides a core set of statistical tools for analyzing, classifying and synthesizing terrains. Here, we first introduce fundamental orometric concepts and notation used throughout the paper and then demonstrate that orometry statistics are effective for mountain characterization in terms of accurately distinguishing between different classes of relief.

4.1 Fundamental concepts

Orometry is a subfield of geography that concentrates on the measurement of mountain and relief features. For our purposes it provides unambiguous definitions of topographical metrics for prominence, dominance, relevance, and isolation, which relate peaks to each other and the saddles between them. In addition a graph structure, known as the Divide Tree, enables the spatial encoding of peak and saddle relationships. As a preliminary to defining these metrics, let the function $h : \Omega \rightarrow \mathbb{R}$ denote the elevation of a point in a domain $\Omega \subset \mathbb{R}^2$. A peak at a location $\mathbf{p} \in \Omega$ is a local maximum of h, with the set of peaks being $\mathcal{P}(\Omega)$.

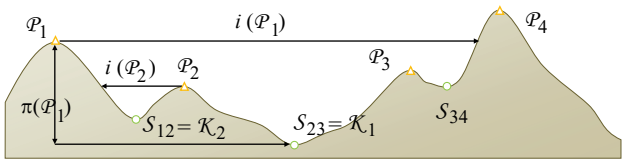

Fig. 3. A diagrammatic representation of peaks $\mathcal{P}$, along with their prominence $\pi(\mathcal{P})$, isolation $i(\mathcal{P})$, and key saddles $\mathcal{K}$. Saddles are also labelled as $\mathcal{S}_{ij}$ according to their adjacent peaks ($\mathcal{P}_i$ and $\mathcal{P}_j$) in the Divide Tree.

The most obvious measure for a peak $\mathcal{P}_i$ is its elevation $h(\mathcal{P}_i)$, but, on its own, this provides a poor characterization, since it fails to incorporate any notion of relative importance, without which highly-localised maxima arising from surface irregularities assume the same stature as true peaks.

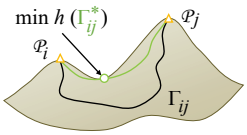

Fig. 4. Two paths connecting peaks $\mathcal{P}_i$ and $\mathcal{P}_j$.

Richer and more informative metrics are therefore warranted [Helman 2005]. In particular, *topographical prominence* $\pi(\mathcal{P}_i)$ measures how important or independent a mountain is relative to other peaks. Widely used in compiling summit lists, it is also useful for distinguishing between principal and secondary peaks [Fry 1987]. It is defined as the shortest vertical distance that must be descended from peak $\mathcal{P}_i$ before being able to reascend towards any other higher peak $\mathcal{P}_j$.

Let Γ_{ij} be a path between peaks $\mathcal{P}_i$ and $\mathcal{P}_j$, and Γ^*_{ij} be any one of the paths that maximizes the minimum elevation along its course,

by passing at its lowest elevation through a saddle (Figure 4). The prominence of a peak $\mathcal{P}_i$ in a given domain $\mathcal{D}$ is then defined as:

$$\pi(\mathcal{P}_i) = h(\mathcal{P}_i) - \max_{\mathcal{D}} \left(\min_{\mathcal{D}} (h(\Gamma^*_{ij})) \right) \quad \forall \mathcal{P}_j,\ h(\mathcal{P}_j) > h(\mathcal{P}_i)$$

An equivalent definition of prominence is the difference in elevation between the peak $\mathcal{P}_i$ and the lowest possible contour encircling $\mathcal{P}_i$ but no other higher peak. By definition, somewhere on this contour there must always exist a saddle $\mathcal{S}$, which is identified as the *key-saddle* of the peak $\mathcal{P}_i$ and denoted as $\mathcal{K}_i$ (Figure 3). In the unlikely case of multiple saddles occurring along the same contour, it is possible to deterministically select one, with the remaining saddles assigned to other peaks. Thus, for any given elevation map, there always exists a unique bijective mapping between key saddles and peaks [Helman 2005]. The prominence for the highest peak of a continent or an island is equal to its elevation; its key saddle is undefined but it can be considered anywhere at sea level.

Given two peaks of equivalent prominence, the one with a higher prominence to elevation ratio will be perceptually more significant. This ratio is called *dominance*:

$$\delta(\mathcal{P}_i) = \pi(\mathcal{P}_i)/h(\mathcal{P}_i)$$

Jurgalski [2016] employs this metric as a way of distinguishing between main peaks, sub-peaks, mountains, and massifs.

Next, we define the relative prominence $\widetilde{\pi}$ and relative elevation $\widetilde{h}$ of a given peak $\mathcal{P}_i \in \mathcal{P}$, over a mountain domain $\mathcal{D}$, as:

$$\widetilde{\pi}(\mathcal{P}_i) = \frac{\pi(\mathcal{P}_i)}{\max\limits_{\mathcal{P}_k \in \mathcal{D}} \pi(\mathcal{P}_k)} \qquad \widetilde{h}(\mathcal{P}_i) = \frac{h(\mathcal{P}_i)}{\max\limits_{\mathcal{P}_k \in \mathcal{D}} h(\mathcal{P}_k)}$$

Given this, the *relevance* $\rho(\mathcal{P}_i)$ of a peak is the geometric mean of the relative prominence $\widetilde{\pi}$ and relative elevation $\widetilde{h}$:

$$\rho(\mathcal{P}_i) = \sqrt{\widetilde{\pi}(\mathcal{P}_i)\,\widetilde{h}(\mathcal{P}_i)}$$

This means that the most relevant peaks are those, among the higher ones, that are also more prominent.

It is important to note that relevance is more strongly influenced by the choice of domain $\mathcal{D}$, and hence which peaks contribute the maximum prominence and elevation, than other metrics.

Finally, the *isolation* $i(\mathcal{P}_i)$ of a peak is the minimum Euclidean distance from $\mathcal{P}_i$ to any higher point on the terrain:

$$i(\mathcal{P}_i) = \min_{\mathbf{p} \in \mathcal{D},\, h(\mathbf{p}) > h(\mathcal{P}_i)} \|\mathbf{p} - \mathcal{P}_i\|$$

From a viewing perspective, the summits of isolated mountains offer the best vantage points since no other peaks occlude the vista. The summit of Everest is the only point on Earth surface with undefined isolation.

Divide Tree. A Surface Network, or Morse-Smale topological representation, captures the critical points and lines of an elevation function h [Čomić et al. 2005]. This Surface Network can be seen as the union of two dual graphs: the Ridge Network composed of the peaks, saddles and ridges, and the River Network defined by the pits, saddles, and channels [Werner 1988].

It is possible to prune the Ridge Network $\mathcal{G}_R$ in two ways. First, by removing the lowest saddle in each cycle and its incident ridges we leave the $n_\mathcal{P}$ peaks and their $n_\mathcal{P} - 1$ key-saddles. Recall that the highest peak in a bounded region does not have a key saddle by definition. This sub-graph, which retains the necessary information for calculating peak prominences and related metrics, is the *Divide Tree* $\mathcal{T}$ of the terrain [Helman 2005], so called because its ridge lines act as separators between watershed regions (see Figure 5). Second, we can include in $\mathcal{T}$ only the peaks above a given prominence threshold ε, as illustrated in Figure 6. Note how the major ridge structures are still present with large ε.

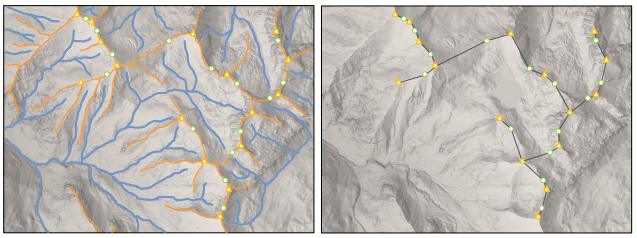

Fig. 5. Left: Surface Network of a DEM, composed of the Ridge (orange) and River (blue) sub-networks. Right: the corresponding Divide Tree for the Ridge Network.

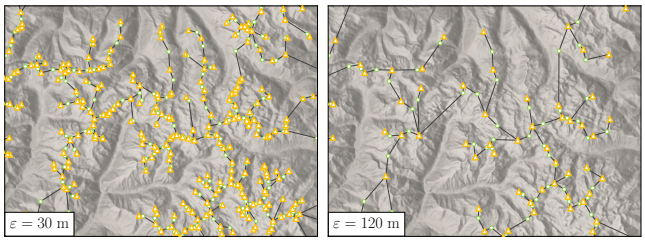

Fig. 6. Two Divide Trees computed on real terrain data at different prominence thresholds showing peaks (orange) and saddles (green).

4.2 Terrain classification

In many instances, mountain ranges in different regions of the world are visually distinct due to differences in their underlying geomorphology, specifically their constituent rock strata and shaping processes. Our hypothesis is that orometry is sufficient to characterize such differences and we test this by training a Random Forest classifier with paired orometric statistics and region labels, and then examining its subsequent classification accuracy.

In our experiments we used a database of peaks and key saddles [Kirmse and de Ferranti 2017] encompassing all the world's summits with prominence greater than 30 m (7.8M peaks), or isolation in excess of 1 km (24.7M peaks).

For our first experiment, we selected 50 regions with significant relief representing a variety of mountainous landscapes, such as major ranges (the Alps, Rockies, Himalayas, and Andes), islands (Japan, New Zealand, and Iceland), deserts (Sahara, Gobi, and Nevada), and glacial geography (Patagonia, Scandinavia, and Alaska).

In order to generate training and validation data each region was sampled with disk domains $\mathcal{D}$ of radius R according to a blue noise distribution constrained to ensure at least a $0.5\,R$ separation between disk centers. Then, from the peaks within a given disk we computed histograms of the orometric statistics outlined in Table 1.

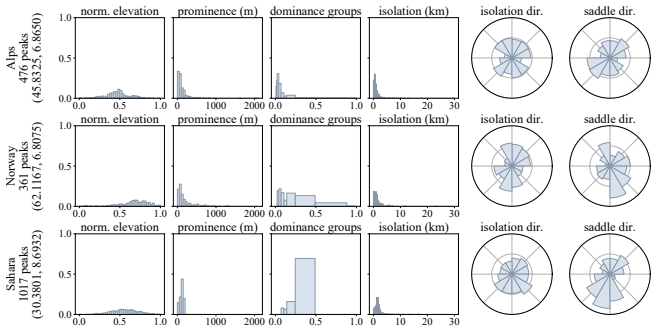

Fig. 7. An orometric histogram analysis of three selected 30 km disk regions, center coordinates (latitude, longitude) are shown on the left side.

Table 1. Orometric features used in our classifier. For the dominance groups, we follow the subdivision of unit interval described in [Jurgalski 2016].

Feature	Metric	Range	#Bins
Dominance	$\delta(\mathcal{P}_i)$	$[0, 1]$	20
Dominance groups	$\delta(\mathcal{P}_i)$	$[0, 1]$	Specific
Normalized elevation	$\hat{h}(\mathcal{P}_i)$	$[0, 1]$	20
Isolation direction	$\nu(\mathcal{P}_i)$	$[0, 360]$	12
Isolation distance	$i(\mathcal{P}_i)/R$	$[0, 1]$	20
Key saddle direction	$\theta(\mathcal{P}_i - \mathcal{K}_i)$	$[0, 360]$	12
Key saddle distance	$\|\mathcal{P}_i - \mathcal{K}_i\|/R$	$[0, 1]$	20
Prominence	$\pi(\mathcal{P}_i)$	$[0, 2000]$	20
Relative prominence	$\widetilde{\pi}$	$[0, 1]$	20
Relevance	$\rho(\mathcal{P}_i)$	$[0, 1]$	20

Figure 7 demonstrates that disparate regions have correspondingly varied histograms. A feature array was then formed by simply concatenating the bins of these histograms and used to train a Random Forest classifier. This was chosen in preference to a neural network due to the relatively limited size of the training set.

For each region we selected up to 100 discs, and partitioned them randomly on each run in an 80 : 20 split between training and validation. Classification accuracy was averaged over 100 runs. Finally, the disk radius R was varied between 10 and 50 km in order to assess its impact on accuracy.

Table 2 shows classification results for different radii taken both overall and according to the contribution of individual features (the corresponding confusion matrix appears in supplementary material). Accuracy generally improves with increasing R, with the highest mean accuracy of 75.3% obtained for $R = 50$ km. Two factors contribute to this limit on overall accuracy. First, because we limit the extent of overlap between disks, fewer than 80 training samples might be available in smaller regions. We found that $R = 30$ provided the best tradeoff between sampling density and accuracy. Second, some of the regions, although geographically dispersed, are actually visually and geomorphologically similar.

This is borne out by a second experiment, in which the classifier is trained on a subset of 15 regions, with a disk radius of 30 km. The overall mean accuracy in this case is 86%. The confusion matrix in Figure 8 shows that the classifier can fail to distinguish between

Table 2. Accuracy of our orometric classifier for 50 regions, averaged over 100 runs and with sampling disk radius varying from 10 km to 50 km. Accuracy is reported both overall and by individual classifier feature.

	10 km	20 km	30 km	40 km	50 km
All, mean acc.	31.5	48.2	61.7	71.0	75.3
All, median acc.	24.0	42.0	61.5	69.5	74.5
Dominance	13.4	20.6	27.7	34.4	38.9
Dominance groups	19.4	28.2	36.7	45.2	47.9
Normalized elevation	5.1	8.4	11.7	15.3	18.0
Isolation direction	5.8	12.0	18.6	25.4	30.1
Isolation distance	10.3	14.8	19.0	23.0	27.1
Key saddle direction	8.2	14.3	21.2	25.8	29.4
Key saddle distance	9.1	13.2	18.0	21.4	24.8
Prominence	7.4	12.8	19.9	27.9	33.1
Relative prominence	9.2	14.7	20.7	25.7	29.8
Relevance	8.1	13.9	19.0	23.9	28.2

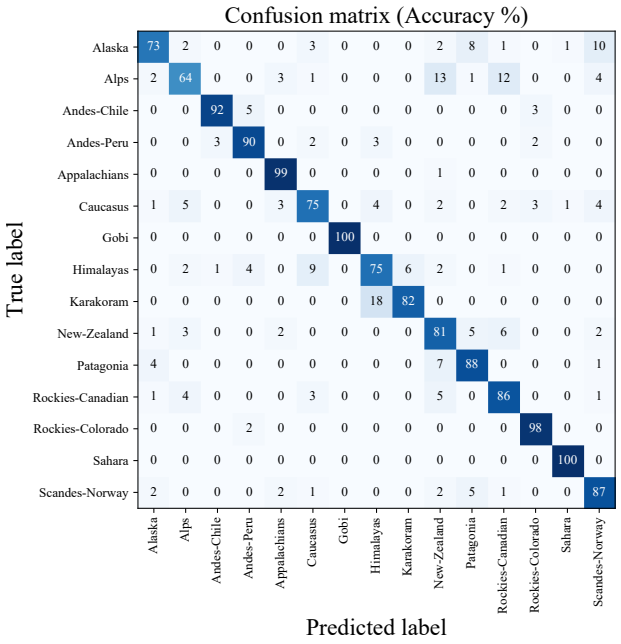

Fig. 8. Confusion matrix for 15 relief regions.

regions with similar underlying geomorphology such as the Alps, New Zealand and the Canadian Rockies. Interestingly, different sections of the same mountain range, such as the Rockies in Canada or Colorado, are not necessarily confused. Even neighboring regions with similar elevation ranges, like the Himalayas and Karakoram, are also properly distinguished.

In conclusion, our experiments demonstrate that orometric statistics are capable of effectively characterizing mountainous regions and can therefore provide a basis for parametrizing the creation of digital terrain belonging to visually distinct classes.

5 DIVIDE TREE GENERATION

We seek to synthesize a terrain that respects the orometric properties of a given terrain type. Rather than attempting to create an elevation map directly, we work initially with a Divide Tree, a vector-based intermediate structure that encapsulates the information required for orometric analysis and matching.

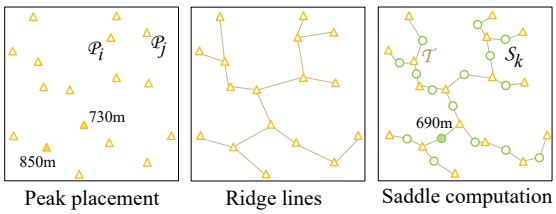

Fig. 9. Divide Tree generation. Peaks are distributed according to the input orometry and connected by ridges to form a graph. Finally, saddles are inserted with their elevation set to fulfill the prominence and dominance constraints of the terrain type.

We present an algorithm for creating a Divide Tree (Fig. 9) that iteratively and successively places peaks, adds connecting ridges, and adjusts the elevation of intermediate saddles, with the aim of matching a given orometric distribution.

5.1 Peaks

The first step involves placing $n_{\mathcal{P}}$ peaks across the target domain $\mathcal{D}$, by assigning an elevation $h(\mathcal{P}_i)$ and position $\mathbf{p} \in \mathcal{D}$ to each. The number of peaks can either be derived from the terrain type density or supplied by the user. The elevations of candidate peaks are sampled from the elevation histogram, and assigned in decreasing order. Individual peaks $\mathcal{P}_i$, starting from the highest, are then placed using dart throwing. The acceptance probability $p(\mathcal{P}_i)$ for position $\mathbf{p}$ depends on the context of previously positioned peaks as they impact the isolation distance $i(\mathcal{P}_i)$ and direction $v(\mathcal{P}_i)$, as well as the user input maps for density C_P and coarse elevation C_H:

$$p(\mathcal{P}_i) = C_P(\mathbf{p}) \cdot n(C_H(\mathbf{p}) - h(\mathcal{P}_i)) \cdot p(i(\mathcal{P}_i)) \cdot p(v(\mathcal{P}_i)),$$

where $n(x)$ is a zero-centered normal distribution with a standard deviation set to 1/20th of the range of C_H that controls the probability of divergence between the actual peak height and the elevation map at $\mathbf{p}$. The terms $p(i(\mathcal{P}_i))$ and $p(v(\mathcal{P}_i))$ are probabilities derived from the corresponding isolation distance and direction histograms in the terrain type.

5.2 Ridge lines

In the second step, we introduce ridge lines that connect pairs of nearby peaks. We note that Divide Trees sourced from real terrains resemble sub-graphs of a Delaunay triangulation, since peaks (vertices) are usually connected based on proximity by ridges (edges) that do not intersect. Our analysis of several Divide Trees confirmed this hypothesis: more than 95% of the peak to peak connections – omitting the intermediate saddle – in $\mathcal{T}$ are edges in the corresponding Delaunay triangulation of the peak positions. Furthermore, previous work in geology showed that the topology of a ridge network often minimizes the total ridge length in fluvial-eroded landscapes [Mark 1981]. Hence, we compute the triangulation of the peak positions and derive a Divide Tree $\mathcal{T}$ as the minimum spanning tree (MST) of this triangulation, with the following edge weights:

$$\omega_{ij} = \frac{\|\mathcal{P}_i - \mathcal{P}_j\|}{\min\left(h(\mathcal{P}_i), h(\mathcal{P}_j)\right)^{\rho}}, \tag{1}$$

This weight is proportional to the distance between peaks, inversely proportional to the lowest of the two peaks in the ridge, and the exponent ρ controls the balance between short (low ρ) and elevated (high ρ) ridges. This control allows us to deviate from the distance-based MST of the peaks ($\rho = 0$) and capture different types of landscapes. In practice, based on empirical observation (see supplementary material for more detail), we set $\rho = 0$, 1, or 2.

Finally, along every ridge $(i, j) \in \mathcal{T}$ we create a saddle $\mathcal{S}_{ij}$ between $\mathcal{P}_i$ and $\mathcal{P}_j$ by randomly splitting the segment and introducing a small perturbation of its planar position.

5.3 Multi-pass placement

While this direct synthesis of peaks and ridges conforms to the provided statistics, it fails to reproduce the hierarchical branching structure of real Divide Trees. This is evident in Figure 6, where a high prominence cutoff leads to a spine of primary ridges, while lowering the threshold adds intermediate peaks and secondary branching ridges. Furthermore, prominence tends to follow an inverse exponential distribution (see Fig. 7).

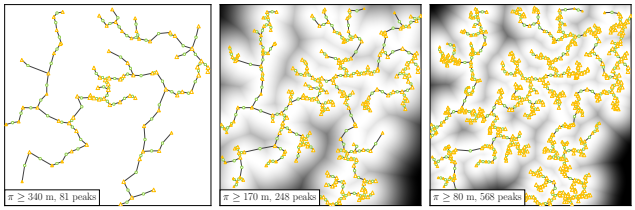

Fig. 10. Multi-pass creation of a divide tree. The background shows C_P, set to 1 for the first step, which takes into account the distance to the ridges of the previous step.

On this basis, we adopt a multi-pass strategy for peak and ridge placement (Figure 10). We assign peaks to prominence bins, such that each subsequent less prominent bin holds twice the number of peaks. Then, we successively place the peaks and ridges for each bin. Already synthesized peaks are propagated to subsequent passes as fixed constraints. We also diffuse the ridges into the probability map C_P so that peaks in subsequent less prominent bins are more likely to be positioned near already synthesized ridges.

5.4 Saddle elevations

The mechanism for assigning elevations to individual saddles is critical because it impacts the pairing between a peak and its key saddle, and consequently the distribution of prominence and dominance values, and all the dependent orometric statistics. Even if peak-saddle pairings do not shift, altitude changes will still affect these distributions. To approximate a target dominance distribution we need to lower saddles from their upper reference

$h^{\max}(\mathcal{S}_{ij}) = \min(h(\mathcal{P}_i), h(\mathcal{P}_j))$ through an optimization process (the same general procedure applies for prominence). We begin by sampling the target dominance distribution to obtain $n_{\mathcal{P}}$ dominance values. Given a target dominance value $\hat{\delta}_j$, we can assign $\delta'(\mathcal{P}_i) = \hat{\delta}_j$ to peak i by modifying its key saddle $\mathcal{K}_i$ elevation:

$$h'(\mathcal{K}_i) = h(\mathcal{K}_i) - h(\mathcal{P}_i) \cdot (\hat{\delta}_j - \delta(\mathcal{P}_i))$$

Therefore, we compute an $n_{\mathcal{P}} \times n_{\mathcal{P}}$ cost matrix M_δ with entries:

$$M_\delta(i,j) = \frac{(h(\mathcal{P}_i) \cdot (\hat{\delta}_j - \delta(\mathcal{P}_i)))^2}{\|\mathcal{P}_a - \mathcal{P}_b\|}$$

if $0 \le h'(\mathcal{K}_i) \le h^{\max}(\mathcal{K}_i)$ and $M_\delta(i,j) = \infty$, otherwise. Here, $\mathcal{P}_a$ and $\mathcal{P}_b$ are the two peaks with ridges directly connected to $\mathcal{K}_i$ in $\mathcal{T}$ (i.e., $\mathcal{K}_i = \mathcal{S}_{ab}$). Recall that $\mathcal{P}_i$ may not be directly ridge-connected to its key saddle $\mathcal{K}_i$ (as illustrated in Figure 3). This formulation of $M_\delta(i,j)$ thus targets the dominance $\hat{\delta}_j$ while penalizing saddles that are deep relative to their neighbouring peaks ($\mathcal{P}_a$ and $\mathcal{P}_b$).

Next, by applying optimal transport [Bonneel et al. 2011] on the cost matrix M_δ, we find the optimal assignment of sampled dominances to peaks and modify the elevation of their key saddles accordingly. For assigning prominence the same procedure applies except that the cost matrix is replaced by:

$$M_\pi(i,j) = \frac{(\hat{\pi}_j - \pi(\mathcal{P}_i))^2}{\|\mathcal{P}_a - \mathcal{P}_b\|}$$

if $0 \le h'(\mathcal{K}_i) \le h^{\max}(\mathcal{K}_i)$ and $M_\pi(i,j) = \infty$ otherwise. Saddle elevations are modified as follows:

$$h'(\mathcal{K}_i) = h(\mathcal{K}_i) - (\hat{\pi}_j - \pi(\mathcal{P}_i))$$

Unfortunately, the very act of adjusting saddle elevations can shift the correspondence between peaks and their key saddles (as shown in Figure 11), thereby discontinuously altering dominance and prominence values and damaging the quality of the distribution match. Rather than rely on a complex constrained optimization solution, we instead apply optimal transport assignment iteratively, alternating between dominance and prominence targets. In practice, we found that this process converges after 3 – 4 iterations.

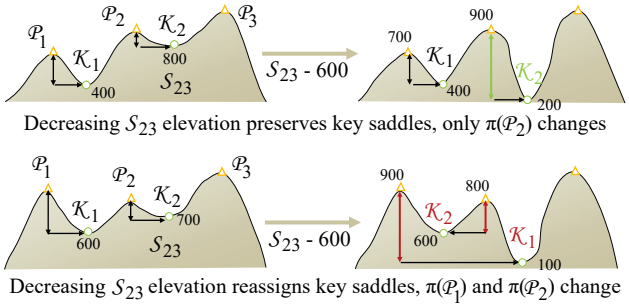

Fig. 11. The impact of adjusting saddle altitudes. The two cases (top left and bottom left) have the same actual and target prominence distributions. The goal is to match the actual (300, 100) and target (300, 700) by altering saddle altitudes. Top right: Adjusting the right saddle downward by 600m achieves the target distribution. Bottom right: The same elevation change swaps the correspondence between peaks and key saddles and leads to a more divergent distribution (800, 200).

6 TERRAIN GENERATION

The challenge lies in synthesizing a dense elevation map $\mathcal{H}$ from a vector-based Divide Tree $\mathcal{T}$, which conveys important but very sparse information (about one sample per 2.5 km^2). Our approach is to generate data that is progressively richer and more dense, by applying the following steps (Figure 12): 1) dual river network computation, 2) sub-sampling and building a triangulated irregular network, 3) multi-scale constrained erosion. This process is constrained by a need to respect the original orometry statistics.

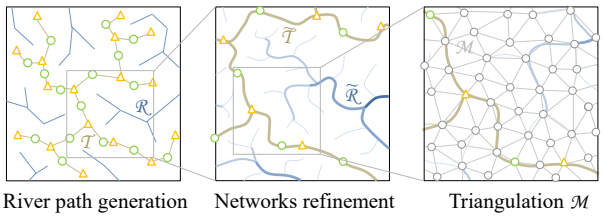

Fig. 12. Overview of the first stages of terrain generation. Given the sparse vector data embedded in the Divide Tree $\mathcal{T}$, a coarse path for the rivers is first generated, then the river and ridge networks are further refined, and, finally, the terrain is resampled with appropriate slope determination.

6.1 River network

The river network $\mathcal{R}$ can be viewed as the dual of the ridge network represented by the input Divide Tree $\mathcal{T}$. To construct it, we compute a Voronoi diagram over the peaks and saddles of $\mathcal{T}$ and prune any edge that would cross a ridge in $\mathcal{T}$ (Figure 12 left).

We can set the maximum elevation of a given river node by using the altitude of the intersection of its incident pruned edge with the ridge network. Then starting from source nodes, easily identified as river nodes of degree 1, we traverse the river graph propagating maximum elevation bounds and in the process building an oriented drainage network. We then refine the river nodes by propagating elevations from tributaries to outlets according to the river slope [Génevaux et al. 2013].

6.2 Refinement and triangulation

The previously computed ridge and river networks are then augmented with a denser sampling (Figure 12 middle). Given a user-defined meshing distance λ (200 m in our implementation), we refine and perturb the geometry of the ridges and rivers to obtain revised networks $\widetilde{\mathcal{T}}$ and $\widetilde{\mathcal{R}}$, respectively.

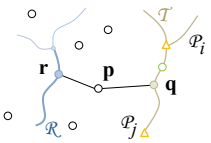

Fig. 13. Computation of a sample's elevation.

In order to do so, we add intermediate points to ridge and river segments such that all edge distances are smaller than λ. A random planar displacement is performed on these intermediate points, whereas their elevation is linearly interpolated along the original segment. A Poisson disk-sampling, with prescribed radius λ, is then used to populate the entire domain. The computed elevation for these samples is derived from the elevations of the closest ridge and river points (see Figure 13).

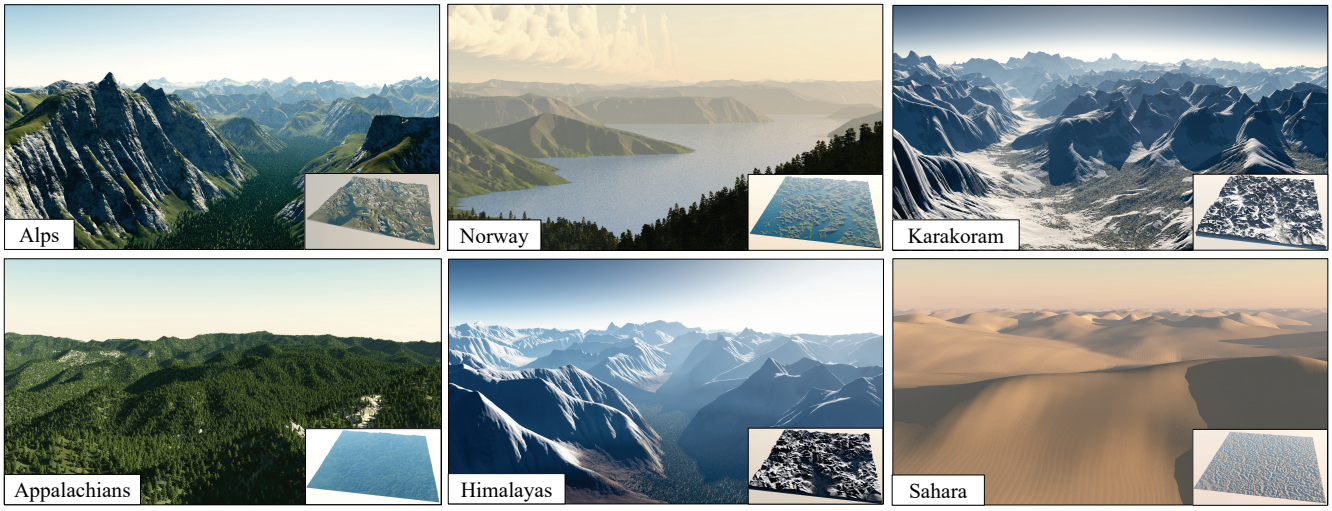

Fig. 14. Our method successfully synthesizes different mountain range forms (the Alps, Fjords, Himalayas, Appalachians, and Karakoram) and can even generate other relief, such as sand dunes (Sahara).

We rely on the power law described in May *et al.* [2013], which approximates the valley width as $w \propto \mathcal{A}^{0.4}$, where $\mathcal{A}$ is the drainage area of a point on the river. Let $\mathbf{q}$ and $\mathbf{r}$ denote the projections of $\mathbf{p}$ onto the Divide Tree $\mathcal{T}$ and the river network $\mathcal{R}$, respectively. If the distance to the river network is below the valley width ($d(\mathbf{p}, \mathcal{R}) < w$) then we set the elevation to that of the river $h(\mathbf{r})$; otherwise, we interpolate between the elevations of the ridge and the river:

$$h(\mathbf{p}) = (1-\alpha)\, h(\mathbf{q}) + \alpha\, h(\mathbf{r}) \qquad \alpha = \frac{d(\mathbf{p}, \mathcal{T})}{d(\mathbf{p}, \mathcal{R}) + d(\mathbf{p}, \mathcal{T}) - w}$$

Finally, we generate a triangulated irregular network representation $\mathcal{M}$ of the terrain, using a constrained Delaunay triangulation that retains existing ridge and river segments.

6.3 Constrained multi-scale erosion

A fully-realized high resolution terrain $\mathcal{H}_0$ is created by augmenting the triangulated terrain $\mathcal{M}$ with multi-fractal noise. The magnitude of the fractal noise is set lower than the prominence threshold ε to guarantee that the orometry of $\mathcal{T}$ is preserved.

As a last step, we perform constrained multi-scale hydraulic erosion in order to introduce gentle sedimentary valleys and erosion landforms, such as ravines and gullies. This is complicated by the need to preserve the elevation of peaks and saddles, and more generally the orometry of $\mathcal{T}$. Our approach is to interleave state-of-the art hydraulic erosion steps [Cordonnier et al. 2017] with procedural uplift. The latter compensates for any unwanted erosion in the neighbourhood of peaks and saddles.

Let $\mathcal{E}_i$ denote the elevation of the terrain after an erosion step. The compensating uplift $\mathcal{U}$ is defined by computing a distance field $d(\mathbf{p}, \mathcal{T})$ centered on the peaks and saddles of the Divide Tree, and applying a fall-off function: $\mathcal{U} = g \circ (d(\mathbf{p}, \mathcal{T})/R)$. Here, R represents a user-defined radius of influence for the peaks and saddles and g is a smooth compactly-supported polynomial of the distance $g(r) = (1-r^2)^3$. Based on this, the elevation update step due to uplift is:

$$\mathcal{H}_{i+1} = \mathcal{E}_i + \mathcal{U} \cdot \Delta\mathcal{H}_i \qquad \Delta\mathcal{H}_i = \mathcal{E}_i - \mathcal{H}_i$$

We applied constrained erosion at three different scales: 100 m, 50 m and 30 m. Terrains showcased in Figure 14 (specifically the Alps, Himalayas and Karakoram) illustrate the results of our approach and visually demonstrate that the orometry is preserved.

7 RESULTS

We implemented our terrain analysis and generation algorithms in Python, with the exception of the multi-resolution erosion, which was coded in C++. Experiments were performed on a desktop computer equipped with an Intel® Core *i*7, clocked at 4 GHz with 16 GB of RAM, and an NVidia GTX 970 graphics card. The output of our system was streamed to e-on Vue® software in order to produce the photorealistic landscape renderings. The average time to generate a $90 \times 90\,\text{km}^2$ terrain at 30 m precision (3000×3000 resolution) ranged from 60 seconds for low peak densities (a Norwegian orometry with around 1000 peaks) up to 190 seconds at the highest density (an Appalachian orometry with more than 2800 peaks).

7.1 Validation

Here, we present several results and applications that highlight key aspects of our synthesis algorithm. First, unlike prior work, our method reproduces a wide variety of terrain archetypes when provided with appropriate orometric distributions. Figure 14 shows six examples of $90 \times 90\,\text{km}^2$ terrains with distinctive visual styles (histograms of the corresponding orometric statistics appear in Figure 7 and the supplementary material).

Our method converges towards the prescribed distributions. Elevations are directly sampled from the input histogram, therefore the discrepancy between distributions is very low if sampled density is similar or larger than the original terrain. Isolation is mainly influenced by the peaks positions from the dart throwing process, and

Fig. 15. A side-by-side comparison between real photographs and generated terrains obtained with our method using orometry from the corresponding region. Karakoram picture by Guilhem Vellut.

the maximum histogram error on the generated terrains is about 8%. Prominence and dominance converged to a maximum error between 2 and 3%. For illustration, Figure 16 shows the effect when we optimize on the same Divide Tree the height of the saddles towards a uniformly distributed histogram of prominences instead of a real distribution, resulting in a non-plausible terrain.

Fig. 16. Different prominence distributions on the same Divide Tree: real (left), and a uniformly distributed (right).

We also tested the correspondence between the real and our synthetic orometry by applying the region classifier (see Section 4.2). In 100 runs of the classifier, our synthesized Sahara, Appalachians and Karakoram are always classified correctly; our Himalayas have a 1% confusion with the real Karakoram; our Norway is confused 11% of the time with the real Patagonia; and only our synthesized Alps exhibit significant misclassification (78% confused with the real Canadian Rockies). In the latter case, this mis-assignment also occurred when we analyzed and classified real datasets (Figure 8), likely because these classes are visually and orometrically similar.

In any event, there is a strong visual similarity as demonstrated by Figures 1 and 15, where we compare real photographs with digital terrains synthesized with matching regional orometry, and Figure 17, where we compare with the real DEM used to compute the distributions.

7.2 Control

One of the major strengths of our synthesis is the flexibility and range of available authoring controls (as showcased in Figure 18). At a broad level, peak placement is guided by a combination of coarse elevation C_H and density C_P maps, which locally control

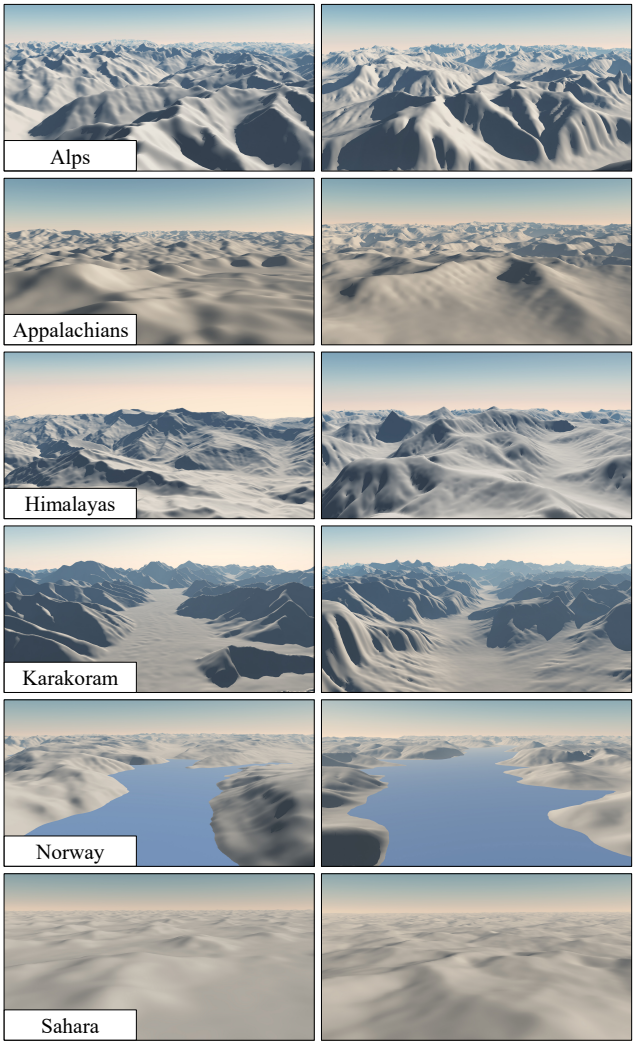

Fig. 17. A side-by-side comparison between real SRTM maps (left) and our synthesis (right) using the corresponding analysed orometry.

the average height of peaks and their probability of occurrence, respectively. It is even possible to demarcate flat areas for seas, lakes and valley floors by zeroing corresponding regions in C_H and C_P. For more fine-grained control, the user can place specific peaks before synthesis, and add, modify or erase features in the Divide Tree after synthesis (see Figure 18). It is also possible to copy and paste portions of a real Divide Tree and auto-complete the surroundings. In Figure 19, we placed the real Divide Tree of Denali and its nearby ridges manually, with the remainder of the $100 \times 100\,\mathrm{km}^2$ terrain synthesized automatically from Alaskan statistics.

In addition, multiple terrain types can coexist in a single terrain, as illustrated in Figure 24. The user provided a type map C_T segmenting the domain into separate terrain types, and during Divide Tree construction this is probed to determine the appropriate orometry for peak placement and saddle elevation optimization. The

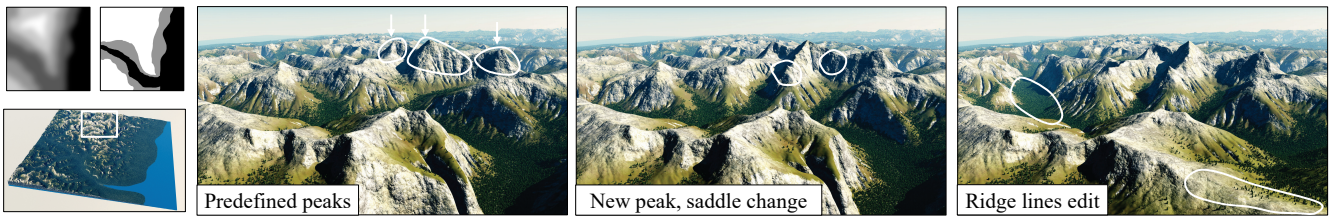

Fig. 18. Stages of an editing session. The left close-up shows the outcome of synthesis with orometry from the Pyrenees, coarse elevation and peak density control maps (on the far left), and three predefined peaks (highlighted). In the middle, a new peak is inserted and a saddle is manually repositioned. Then, on the right, an entire ridge is deleted to reshape the valleys. Please refer to the video for more details.

Divide Tree is fused together during ridge line Delaunay triangulation, which is independent of C_T. This combination of high-level authoring and precise control is crucial in an artistic pipeline, and is a weakness of many previous methods.

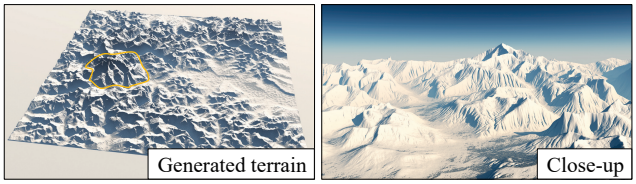

Fig. 19. Stitching in a Divide Tree. A Divide Tree is extracted from around Denali (highlighted) and inserted into the domain. Given this real tree fragment, a user-drawn coarse elevation map (inset), and orometric statistics for Alaska, our synthesis seamlessly completes the rest of the terrain.

Finally, the histograms of each metric can be directly edited to obtain a desired, possibly imaginary, terrain: the Rockies with peaks that are twice as prominent or Saharan dunes ranging in height from 4000 m to 5000 m, for example.

7.3 Comparison with other techniques

To our knowledge, our model is the first to capture such a wide variety of landscapes. Most existing methods either focus on generic Alpine terrains or specific landforms, such as canyons. In contrast, our method spans the gamut from rolling Saharan dunes to serrated Himalayan ranges. Our orometric encoding is also more compact than other vector-based representations, with a $90 \times 90\,\mathrm{km}^2$ terrain typically consisting of 1200-2000 peaks and an equal number of saddles. For comparison, Genevaux *et al.* [2013] and Cordonnier *et al.* [2016] use $10 - 160\,\mathrm{k}$ samples for similarly-sized terrains.

Other approaches that target large spatial scales either do not reproduce truly coherent global structure (e.g., procedural noise and texture synthesis) or suffer from limitations in achievable variety (e.g., tectonic uplift and fluvial erosion). Furthermore, our method scales with the number of peaks rather than the size or resolution of the terrain. Given a Divide Tree, we can later generate a heightfield at any desired output resolution.

We compared our work to the adversarial expansion network proposed in [Zhou et al. 2018]. This method learns from a single exemplar map and uses a guidance image similar to our approach (Figure 21). We trained the network using the authors' provided code and hyper-parameters with a $90 \times 90\,\mathrm{km}^2$ crop from the SRTM 3 arc-second of the Alps. Visually, the produced elevation map contains repetitions and grid artifacts. Analytically, the number of peaks is 7 times too large, the Earth Mover's Distance of the distributions with respect to the input is between 20 and 50% higher than our synthesis, and the elevations histogram is 20 times larger. Consequently, the terrain is always misclassified.

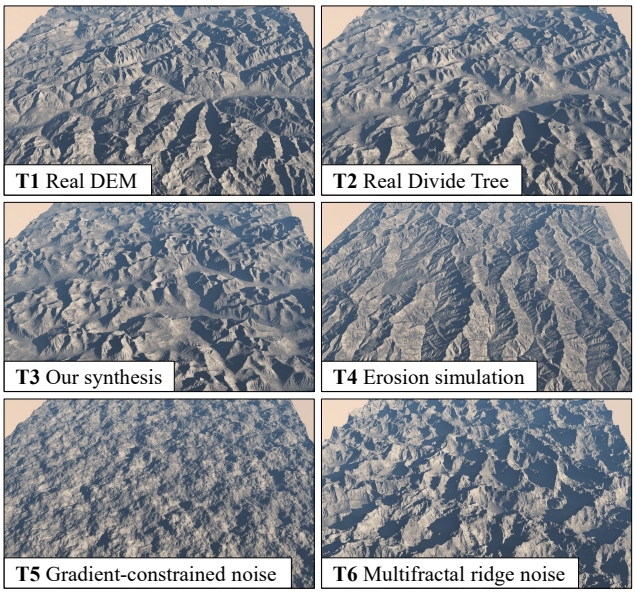

Fig. 20. Comparison between our method, real data and other terrain synthesis approaches as shown in the user study.

The sketch-to-terrain cGAN proposed by [Guérin et al. 2017] offers a more guided terrain synthesis approach, as we can feed the network with the Divide Tree as the input sketch and properly encode the elevation of peaks and saddles. We trained this network using several DEM and their corresponding Divide Tree, cropped from SRTM-3 of the Alps. We used our synthesized Divide Tree as input to create a full elevation map, thus replacing our terrain synthesis pipeline (Section 6). While the overall structure of the Divide Tree is respected, the output terrain contains twice as many peaks, *i.e.* the network is creating new elements affecting the orometric distributions. In contrast, our generation algorithm guarantees that these properties are respected.

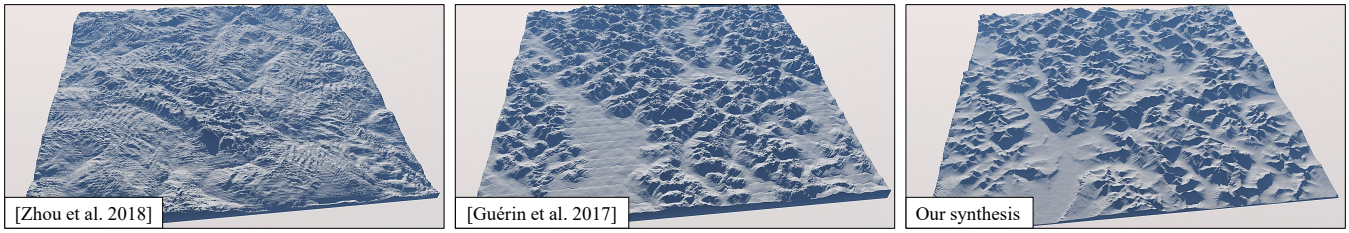

Fig. 21. Comparison between our method and deep learning approaches.

7.4 Perceptual study

As a summative evaluation we conducted a perceptual study to test the perceived realism of our method in comparison with 5 other approaches. The treatments were mountainous terrains obtained from: (T1) a real SRTM-derived DEM from the Alps at 1 arc-second resolution; (T2) our terrain generator (Section 6) with the Divide Tree of the real Alps DEM as input; (T3) our full pipeline (Sections 4–6) with orometry derived from the real DEM; (T4) simulation of uplift and hydraulic erosion [Cordonnier et al. 2016]; (T5) Perlin noise constrained to a distribution of gradients from the real DEM [Parberry 2015]; and (T6) multi-fractal ridged noise [Galin et al. 2019]. All terrains had the same extent: 90×90 km at a sampling resolution of 30 m. Our goal was to have participants evaluate the structural realism of the terrains, so we rendered them from an aerial perspective (Figure 20). Regarding the choice of parameters, T3 used a very coarse elevation map smoothed from a real DEM and uniform probability map. T4 was provided by the authors of [Cordonnier et al. 2016] in their results. T5 uses a gradients distribution analyzed from Southern Utah and was computed using the code and default parameters provided by the author. T6 is a standard sum of ridge fractal noise [Galin et al. 2019].

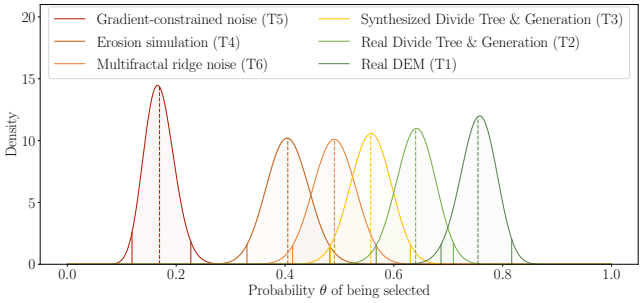

Fig. 22. Results of a forced-choice perceptual study comparing 6 terrain approaches and showing posterior beta distributions, mean values (dashed line) and the 95% credible intervals.

The study was designed as a two-alternative forced choice (2-AFC) task in which subjects were presented with 15 pairs of images in a randomized order and, for each pair, instructed to select the one they regarded as more realistic. The experiment was deployed on a website and posted in a mountaineering forum, and 65 subjects participated. We then performed a Bayesian analysis with the probability of a particular treatment being chosen modeled as a Bernoulli random variable with probability θ and uniform beta prior. Figure 22 shows the posterior distributions for θ. Two extrema are immediately identifiable, corresponding to Parberry's constrained Perlin noise (T5) and the real SRTM DEM (T1). Among the fully synthetic terrains (T3–T6), none of their 95% credible intervals for θ overlap with that of the real DEM (T1) and only our method (T3) overlaps with the heightfield generated from the real Divide Tree (T2). We believe these results indicate that orometric distributions play an important role in the overall perception of terrain.

7.5 Limitations

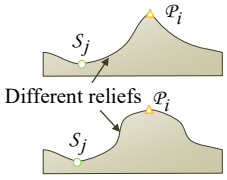

Fig. 23. Differently shaped mountains with the same local Divide Tree.

Although the Divide Tree is a powerful, sparse, and compact data structure for analyzing and generating terrains, it only provides coarse information about the local relief. Certain important structural details are discarded, such as slope profiles (see Figure 23) and the subsidiary ridge network where peak prominences fall below the analysis threshold.

Depending on how local terrain features are realised there are many possible terrains that match a given Divide Tree. We make the assumption that rivers follow the medial axis between ridges, and that ridges themselves drop roughly linearly from peak to saddle. There is room to improve visual realism by extending our analysis and synthesis to incorporate local characteristics, such as ridge and valley profiles.

Furthermore, there remains a gap between real and synthesized Divide Trees as is evident from the perceptual disparity between the real $\mathcal{T}$ (T2) and synthesized $\mathcal{T}$ (T3) in our perceptual study (see Figure 22). Our peak and saddle statistics do not explicitly encode aspects of tree topology such as the degree of vertices and branching depth. It would therefore be worth exploring deeper metrics on real Divide Trees and how these might correlate with orometric measurements and thus inform our synthesis.

8 CONCLUSION

We introduce for the first time the formalism of orometry to the field of computer graphics. Orometry involves measuring mountains and the spatial arrangement of peaks using several metrics, such as prominence, relevance and isolation. These metrics are effective in the automatic classification of mountainous terrains from around

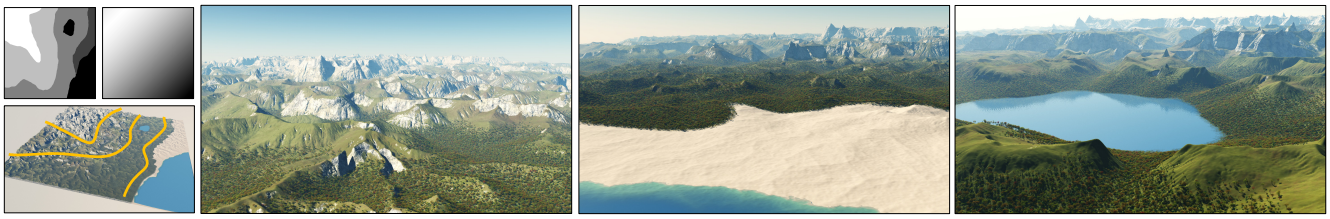

Fig. 24. A terrain generated by combining four different classes from the Sahara, Appalachians, Alps and Peruvian Andes.

the world. Derived from this notion of orometry is the Divide Tree construct, which is a graphical network representation of the position and relationship between peak and saddle points on a terrain. This graph turns out to be a concise yet powerful representation of terrain. We introduce a method to synthesize new Divide Trees that satisfy orometric measures and a matching process to automatically generate the associated terrain. Our method also supports a combination of general and specific authoring tools. The end result is a versatile terrain generation method that is able to produce a broad range of terrain types, from gentle hills to sharp ridges and peaks.

One possible avenue for future work is to incorporate different mountain shapes and valley profiles. In this regard, it might be possible to adapt existing continuous DEM steepness metrics [Earl and Metzler 2015]. Another idea would be to build a dictionary of Divide Tree fragments and then synthesize new terrains by stitching Divide Trees together and applying our terrain generation algorithm.

ACKNOWLEDGMENTS

This work is part of the project *PAPAYA* funded by the *Fonds National pour la Société Numérique* and the project HDW ANR-16-CE33-0001, supported by Agence Nationale de la Recherche. We would like to credit E-on software for providing Vue for rendering our terrain models.

REFERENCES

Sawsan AlHalawani, Yong-Liang Yang, Peter Wonka, and Niloy J. Mitra. 2014. What Makes London Work Like London? *Computer Graphics Forum* 33, 5 (2014), 157–165.

Oscar Argudo, Carlos Andujar, Antonio Chica, Eric Guérin, Julie Digne, Adrien Peytavie, and Eric Galin. 2017. Coherent multi-layer landscape synthesis. *The Visual Computer* 33, 6 (2017), 1005–1015.

Farès Belhadj. 2007. Terrain modeling: a constrained fractal model. In *Proceedings of the International Conference on Computer Graphics, Virtual Reality, Visualisation and Interaction in Africa*. ACM, Grahamstown, South Africa, 197–204.

Nicolas Bonneel, Michiel van de Panne, Sylvain Paris, and Wolfgang Heidrich. 2011. Displacement Interpolation Using Lagrangian Mass Transport. *ACM Transactions on Graphics* 30, 6 (Dec. 2011), 158:1–158:12.

Lidija Čomić, Leila De Floriani, and Laura Papaleo. 2005. Morse-Smale Decompositions for Modeling Terrain Knowledge. In *Spatial Information Theory*, Anthony G. Cohn and David M. Mark (Eds.). Springer, Berlin, Heidelberg, 426–444.

Guillaume Cordonnier, Jean Braun, Marie-Paule Cani, Bedrich Benes, Eric Galin, Adrien Peytavie, and Eric Guérin. 2016. Large Scale Terrain Generation from Tectonic Uplift and Fluvial Erosion. *Computer Graphics Forum* 35, 2 (2016), 165–175.

Guillaume Cordonnier, Eric Galin, James Gain, Bedrich Benes, Eric Guérin, Adrien Peytavie, and Marie-Paule Cani. 2017. Authoring Landscapes by Combining Ecosystem and Terrain Erosion Simulation. *ACM Transactions on Graphics* 36, 4 (2017), 134:1–134:12.

Edward Earl and David Metzler. 2015. Cloud-Capped Towers: Capturing Terrain Characteristics Using Topographic Functionals. *Quaestiones Geographicae* 34, 4 (December 2015), 7–23.

Anna Frühstück, Ibraheem Alhashim, and Peter Wonka. 2019. TileGAN: Synthesis of Large-Scale Non-Homogeneous Textures. *ACM Transactions on Graphics (Proceedings of SIGGRAPH)* 38, 4 (2019), 58:1–58:11.

Steve Fry. 1987. Defining and sizing-up mountains. *Summit, Jan.-Feb.* (1987), 16–21,32.

James Gain, Bruce Merry, and Patrick Marais. 2015. Parallel, Realistic and Controllable Terrain Synthesis. *Computer Graphics Forum* 34, 2 (2015), 105–116.

James E. Gain, Patrick Marais, and Wolfgang Strasser. 2009. Terrain sketching. In *Proceedings of the Symposium on Interactive 3D Graphics and Games*. ACM, Boston, USA, 31–38.

Eric Galin, Eric Guérin, Adrien Peytavie, Guillaume Cordonnier, Marie-Paule Cani, Bedrich Benes, and James Gain. 2019. A Review of Digital Terrain Modeling. *Computer Graphics Forum (proceedings of Eurographics 2019 STAR)* 38, 2 (2019), 553–577.

Jean-David Génevaux, Éric Galin, Eric Guérin, Adrien Peytavie, and Bedrich Benes. 2013. Terrain Generation Using Procedural Models Based on Hydrology. *ACM Transactions on Graphics*. 32, 4 (2013), 143:1–143:13.

Jean-David Génevaux, Éric Galin, Adrien Peytavie, Éric Guérin, Cyril Briquet, François Grosbellet, and Bedrich Benes. 2015. Terrain Modeling from Feature Primitives. *Computer Graphics Forum* 34, 6 (2015), 198–210.

Eric Guérin, Julie Digne, Eric Galin, and Adrien Peytavie. 2016. Sparse representation of terrains for procedural modeling. *Computer Graphics Forum (Proceedings of Eurographics)* 35, 2 (2016), 177–187.

Éric Guérin, Julie Digne, Éric Galin, Adrien Peytavie, Christian Wolf, Bedrich Benes, and Benoît Martinez. 2017. Interactive Example-based Terrain Authoring with Conditional Generative Adversarial Networks. *ACM Transactions on Graphics* 36, 6 (2017), 228:1–228:13.

Adam Helman. 2005. *The Finest Peaks. Prominence and Other Mountain Measures*. Trafford Publishing.

Houssam Hnaidi, Éric Guérin, Samir Akkouche, Adrien Peytavie, and Éric Galin. 2010. Feature based terrain generation using diffusion equation. *Computer Graphics Forum* 29, 7 (2010), 2179–2186.

Eberhard Jurgalski. 2016. Das erweiterte Prominenzkonzept. Ein mathematisches Einteilungssystem für alle Berge und Gebirge, weltweit anwendbar vom Hochgebirge bis zu Heimathügeln. *Mitteilungen der Fränkischen Geographischen Gesellschaft* 61/62 (2016), 105–110.

Alex D. Kelley, Michael C. Malin, and Gregory M. Nielson. 1988. Terrain simulation using a model of stream erosion. *Computer Graphics* 22, 4 (1988), 263–268.

Andrew Kirmse and Jonathan de Ferranti. 2017. Calculating the prominence and isolation of every mountain in the world. *Progress in Physical Geography: Earth and Environment* 41, 6 (2017), 788–802.

Benoit B. Mandelbrot. 1982. *The Fractal Geometry of Nature*. W. H. Freeman & Co Ltd.

David M. Mark. 1981. Topology of ridge patterns: Possible physical interpretation of the "minimum spanning tree" postulate. *Geology* 9, 8 (08 1981), 370–372.

Christine May, Josh Roering, L Eaton, and Burnett Kelly. 2013. Controls on valley width in mountainous landscapes: The role of landsliding and implications for salmonid habitat. *Geology* 41 (03 2013), 503–506.

Forest Kenton Musgrave, Craig E. Kolb, and Robert S. Mace. 1989. The synthesis and rendering of eroded fractal terrains. *Computer Graphics* 23, 3 (1989), 41–50.

Ian Parberry. 2014. Designer Worlds: Procedural Generation of Infinite Terrain from Real-World Elevation Data. *Journal of Computer Graphics Techniques* 3, 1 (2014), 74–85.

Ian Parberry. 2015. Modeling Real-World Terrain with Exponentially Distributed Noise. *Journal of Computer Graphics Techniques* 4, 2 (2015), 1–9.

Przemyslaw Prusinkiewicz and Marc Hammel. 1993. A fractal model of mountains with rivers. In *Proceedings of Graphics Interface*. Canadian Information Processing Society, Toronto, Canada, 174–180.

Christian Werner. 1988. Formal Analysis of Ridge and Channel Patterns in Maturely Eroded Terrain. *Annals of the Association of American Geographers* 78, 2 (1988), 253–270.

Howard Zhou, Jie Sun, Greg Turk, and James M. Rehg. 2007. Terrain Synthesis from Digital Elevation Models. *Transactions on Visualization and Computer Graphics* 13, 4 (2007), 834–848.

Yang Zhou, Zhen Zhu, Xiang Bai, Dani Lischinski, Daniel Cohen-Or, and Hui Huang. 2018. Non-stationary Texture Synthesis by Adversarial Expansion. *ACM Transactions on Graphics (Proceedings of SIGGRAPH)* 37, 4 (2018).